A Facile and Modular Method to Assemble Three-Dimensional DNA Structures

Christopher K. McLaughlin, Graham D. Hamblin, Faisal A. Aldaye, Hua Yang, and Hanadi F. Sleiman*[a]

Department of Chemistry, McGill University, 801 Sherbrooke St. West, Montreal, QC H3A-2K6,Canada

Supplementary Information

Table of Contents

I	General	1
II	Instrumentation	2
III	Oligonucleotides prepared for 2D and 3D constructs	2
IV	Assembly of 2D Polygons	5
V	Preparation of 3D DNA Prisms	7
VI	Characterization of 3D constructs using selective enzymatic digestions	10
VII	Characterization of Cooperativity in 3D Assembly	11
VIII	Increasing Symmetry Elements in 3D DNA Assembly	15
IX	References	19

I. General

StainsAll®, acetic acid, tris(hydroxymethyl)-aminomethane (Tris), formamide and urea were used as purchased from Aldrich. Acetic acid, and boric acid were purchased from Fisher Scientific and used without further purification. Nucleoside (dA,T,dC,dG) derivatized 500 Å and 1000Å LCAA-CPG supports with loading densities between 25-40 μmol/g, 5-ethylthiotetrazole, 1,6-hexanediol phosphoramidite and reagents used for automated DNA synthesis were purchased from ChemGenes Incorporated. Sephadex G-25 (super fine, DNA grade) was purchased from Amersham Biosciences. Mung Bean Nuclease (MBN, source: Mung Bean Sprouts) and Exonuclease VII (ExoVII, source: recombinant) were purchased from BioLynx Incorporated.

1xTB buffer is composed of 0.09M Tris and Boric acid (TB) with a pH ~8.3. 1xTAEMg buffer is composed of 45 mM Tris, 12.5 mM $Mg(OAc)_2 \cdot 6H_2O$ and 2 mM EDTA. The pH was adjusted to 8 using glacial acetic acid.

II. Instrumentation

Standard automated oligonucleotide solid-phase synthesis was performed on a Perspective Biosystems Expedite 8900 DNA synthesizer or Mermade MM6 synthesizer from Bioautomation. Gel electrophoresis experiments were carried out on an acrylamide 20 X 20 cm vertical Hoefer 600 electrophoresis unit. Enzymatic digestions were conducted using a Flexigene Techne 60 well thermocycler.

III. Oligonucleotides prepared for 2D and 3D DNA constructs

General Procedure for Solid-Phase DNA Synthesis:

DNA synthesis was performed on a 1 μmole scale, starting from the required nucleotide modified 500Å or 1000 Å LCAA-CPG solid-support. Additionally, a 1,6 hexanediol phosphoramidte (**C6**) was site-specifically incorporated into each sequence and coupled onto the growing oligonucleotide chain as an artificial base with a prolonged coupling time of 5min. The coupling efficiency was monitored after trityl removal. All sequences were fully deprotected in concentrated ammonium hydroxide (55 ^{o}C, 16 hours).

Table S1: Oligonucleotides prepared via solid-phase synthesis. A hexane (**C6**) spacer was site-specifically incorporated into select sequences using a commercially available phosphoramidite.

Name	Sequence (5′ → 3′)
T1a	TCTAGGAGAC**C6**GTCCAGACTC**C6**CTTTCAACTT
T1b/S1b/P1b/H1b	AAGTTGAAAG**C6**CCGCCGATTA**C6**GTGATGTCAT
T1c/S1c	ATGACATCAC**C6**CCGCCGATTA**C6**GTCTCCTAGA
S1a/P1a/H1a	AGGTTTGCTG**C6**CCGCCGATTA**C6**CTTTCAACTT
S1d/P1d/H1d	TCTAGGAGAC**C6**CCGCCGATTA**C6**CAGCAAACCT
P1c/H1c	ATGACATCAC**C6**CCGCCGATTA**C6**TTCGTCACTA
P1e	TAGTGACGAA**C6**CCGCCGATTA**C6**GTCTCCTAGA
H1e	CGAGTGTCAG**C6**CCGCCGATTA**C6**GTCTCCTAGA
H1f	TAGTGACGAA**C6**CCGCCGATTA**C6**CTGACACTCG
T2a	TCTAGGAGAC**C6**GAAACGACAA**C6**CTTTCAACTT

T2b/S2b/P2b/H2b	AAGTTGAAAG**C6**GAAACGACAA**C6**GTGATGTCAT
T2c/S2c	ATGACATCAC**C6**GAAACGACAA**C6**GTCTCCTAGA
S2a/P2a/H2a	AGGTTTGCTG**C6**GAAACGACAA**C6**CTTTCAACTT
S2d/P2d/H2d	TCTAGGAGAC**C6**GAAACGACAA**C6**CAGCAAACCT
P2c/H2c	ATGACATCAC**C6**GAAACGACAA**C6**TTCGTCACTA
P2e	TAGTGACGAA**C6**GAAACGACAA**C6**GTCTCCTAGA
H2e	CGAGTGTCAG**C6**GAAACGACAA**C6**GTCTCCTAGA
H2f	TAGTGACGAA**C6**GAAACGACAA**C6**CTGACACTCG
H1aT10	AGGTTTGCTG**C6**TTTTTTTTTT**C6**CTTTCAACTT
H1bT10	AAGTTGAAAG**C6**TTTTTTTTTT**C6**GTGATGTCAT
H1dT10	TCTAGGAGAC**C6**TTTTTTTTTT**C6**CAGCAAACCT
H1fT10	TAGTGACGAA**C6**TTTTTTTTTT**C6**CTGACACTCG
T3a	TCTAGGAGAC**C6**GTCCAGACTC**C6**CTTTCAACTT
T3b	AAGTTGAAAG**C6**GTCCAGACTC**C6**GTGATGTCAT
T3c	ATGACATCAC**C6**GTCCAGACTC**C6**GTCTCCTAGA
LS1	TAATCGGCGG**C6**TTATTAAAGTCTCAG**C6**TTGTCGTTTC
$LS_{y'1}$	TAATCGGCGG**C6**TTATTAAAGTCTCAG**C6**TTGTAGTTTC
$LS_{y'2}$	TAATCGGCGG**C6**TTATTAAAGTCTCAG**C6**TTGTACTTTC
LS2	TAATCGGCGG**C6**TTATTAAAGTCTCAG**C6**TAATCGGCGG
LS3	TTGTCGTTTC**C6**TTATTAAAGTCTCAG**C6**TTGTCGTTTC
LS4	GAGTCTGGAC**C6**TTATTAAAGTCTCAG**C6**GAGTCTGGAC
RS	CTGAGACTTTAATAA

Purification:

Crude products were purified on 15% polyacrylamide/8M urea polyacrylamide gels (PAGE; up to 20 OD_{260} of crude DNA per gel) at constant current of 30 mA for 2 hours, using 0.09M Tris-Boric acid (TB) buffer (pH 8.3). Following electrophoresis, the plates were wrapped in plastic and placed on a fluorescent TLC plate and illuminated with a UV lamp (254nm). The bands were quickly excised, and the gel pieces were crushed and incubated in 10 mL of sterile water at 55 ^{o}C for 16 hours. Samples were then dried to 1.5 mL, desalted using size exclusion chromatography (Sephadex G-25), and quantified (OD_{260}) using UV-vis spectroscopy.

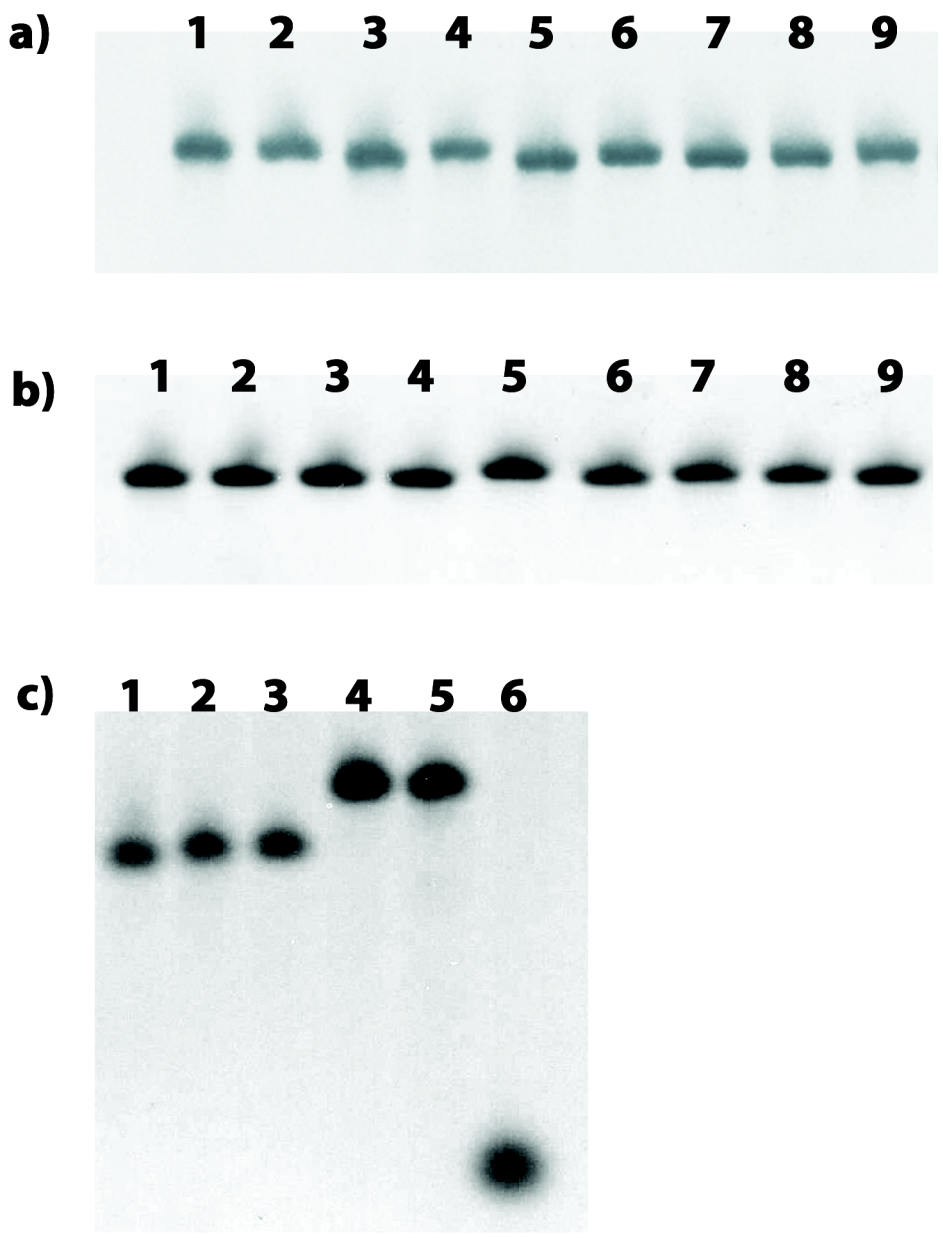

Fig. S1 Denaturing PAGE Analysis of synthesized oligonucleotides. Each experiment (a-c) is a 15% PAGE gel ran for 30 minutes at 250V and then 45 minutes at 500 V. a) Lane 1-T1a, Lane 2-T1b/S1b/P1b/H1b, Lane 3-T1c/S1c, Lane 4-S1a/P1a/H1a, Lane 5- S1d/P1d/H1d, Lane 6-P1c/H1c, Lane 7- P1e, Lane 8- H1e, Lane 9 - H1f. b) Lane 1-T2a, Lane 2-T2b/S2b/P2b/H2b, Lane 3-T2c/S2c, Lane 4-S2a/P2a/H2a, Lane 5- S2d/P2d/H2d, Lane 6- P2c/H2c, Lane 7- P2e, Lane 8- H2e, Lane 9 – H2f. c) Lane 1-T3a, Lane 2- T3b, Lane 3-Tc, Lane 4-LS1, Lane 5- LS2, Lane 6-RS.

IV. Assembly of 2D Polygons

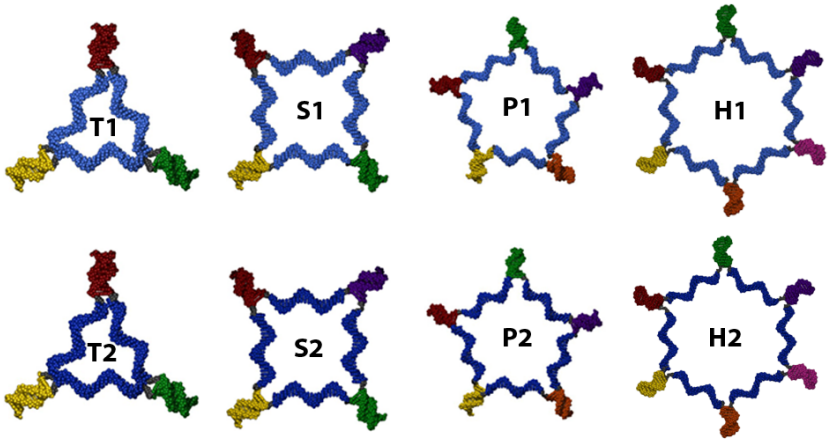

Fig. S2 Schematic representation of 2D geometries required for prismatic 3D DNA construction.

As shown in Fig. S2, the coloured duplex regions for each set of 2D geometries (red, yellow, green –**T1**, **T2** , red, yellow, green, purple-**S1**, **S2** and red, yellow, green, purple, orange-**P1**, **P2**) are an identical set of sequences. By making the sets of templating strands for the formation of each 2D geometry equal, the number of unique base-pairs required to prepare **TP**, **RP**, and **PP** is reduced significantly without affecting sequence unique regions found in each prismatic face. To characterize the assembly pathway of 2D polygons **T1**, **S1**, **P1**, and **H1**, component strands were added in a sequential manner to produce intermediate structures that could be analyzed by PAGE under native conditions (Fig. S3). As an example, equimolar amounts of each building block (6.7 $x10^{-12}$ moles), **T1a-c**, were added together at room temperature in 1xTAEMg buffer to form discrete products (Fig. S3a). In each example, addition of successive component strands generated a discrete intermediate that results from the bi-molecular interaction of the 10 base sequences that act to 'clip' the vertices of each 2D polygon together. These structures are retarded in mobility compared to the previous intermediate, indicating successful hybridization of the 10 base-pair duplexes. Addition of the final component strand – Fig.S3a- Lane 3, produced the desired cyclic polygon **T1** in a quantitative fashion. After confirming the assembly, stock solutions of **T1** could be easily made by taking 0.70 nmoles of each strand **T1a-c** and adding them together with 10 uL of 10xTAEMg buffer and giving a 10 minute hybridization time before use. The total volume was adjusted to 100 µL with autoclaved ultrapure water to give a final **T1** concentration of 7 µM. In a similar fashion, equimolar amounts of each building block (6.7 $x10^{-12}$ moles), **S1a-d**, **P1a-e**, and **H1a-f**, were added together at room

temperature in 1xTAEMg buffer to form discrete products (Fig. S3, b-d, respectively). Structures **T2**, **S2**, **P2** and **H2** showed similar behaviour and stock solutions of all polygons were prepared at 7 μM. Structures are left for 5 minutes at room temperature and then are ready for use.

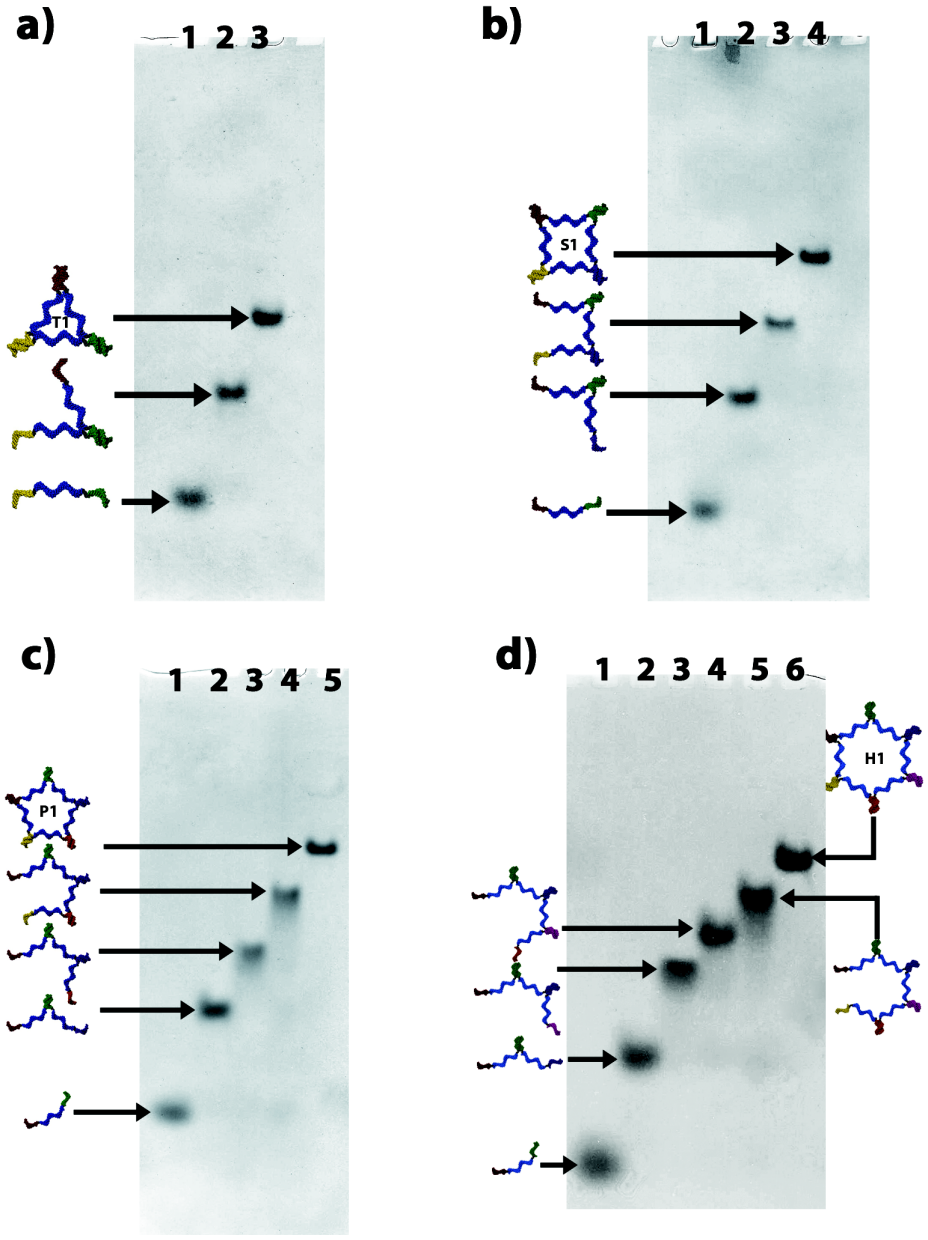

Fig. S3 Sequential assembly and PAGE analysis of T1, S1, P1 and H1. a) Lane 1- T1a, Lane 2- T1aT1b, Lane 3- T1aT1bT1c. **b)** Lane 1- S1a, Lane 2- S1aS1b, Lane 3- S1aS1bS1c, Lane 4- S1aS1bS1cS1d. **c)** Lane 1- P1a, Lane 2- P1aP1b, Lane 3- P1aP1bP1c, Lane 4- P1aP1bP1cP1d, Lane 5- P1aP1bP1cP1dP1e. **d)** Lane 1- H1a, Lane 2- H1aH1b, Lane 3- H1aH1bH1c, Lane 4- H1aH1bH1cH1d, Lane 5- H1aH1bH1cH1dH1e and Lane 6- H1aH1bH1cH1dH1eH1f.

V. Preparation of 3D DNA Prisms

As described in the previous section, each 2D polygon was prepared as a 7 μM stock solution in 1xTAEMg buffer. Stock solutions of both linking strand *LS1* and *RS* were prepared in 1xTAEMg buffer, but at concentrations of 21 μM, 28 μM, 35 μM, and 42 μM. As an example, the step-wise 3D assembly of **TP** (Fig. S4a) was achieved by taking 1 μL of **T1** (7 μM) (Fig S4a, Lane 1) and adding 1 μL of *LS1* (21 μM). After a 3-5 minute wait time at room temperature, the triangle is pre-loaded with 3 linking strands (Fig. S4a, Lane 2) now ready for binding with the second polygon. The second triangle **T2** (1 μL, 7 μM) was then added to the mixture, with an additional 3-5 minute wait time, to generate the single-stranded 3D prism **ssTP** (Fig. S4a, Lane 3). Finally, the intervening sequences were made double-stranded by addition of *RS* (1 μL, 21 μM) to generate 3D prism **TP** (Fig. S4a, Lane 4). Prismatic structures **RP** (Fig. S4b) and **PP** (Fig. S4c) were generated using a similar protocol, except *LS1*/*RS* stock solutions of 28 μM and 35 μM were used, respectively, to maintain stoichiometric ratios. 3D structures are left for 5 minutes after addition of the polygons and linking strands, then are ready for use.

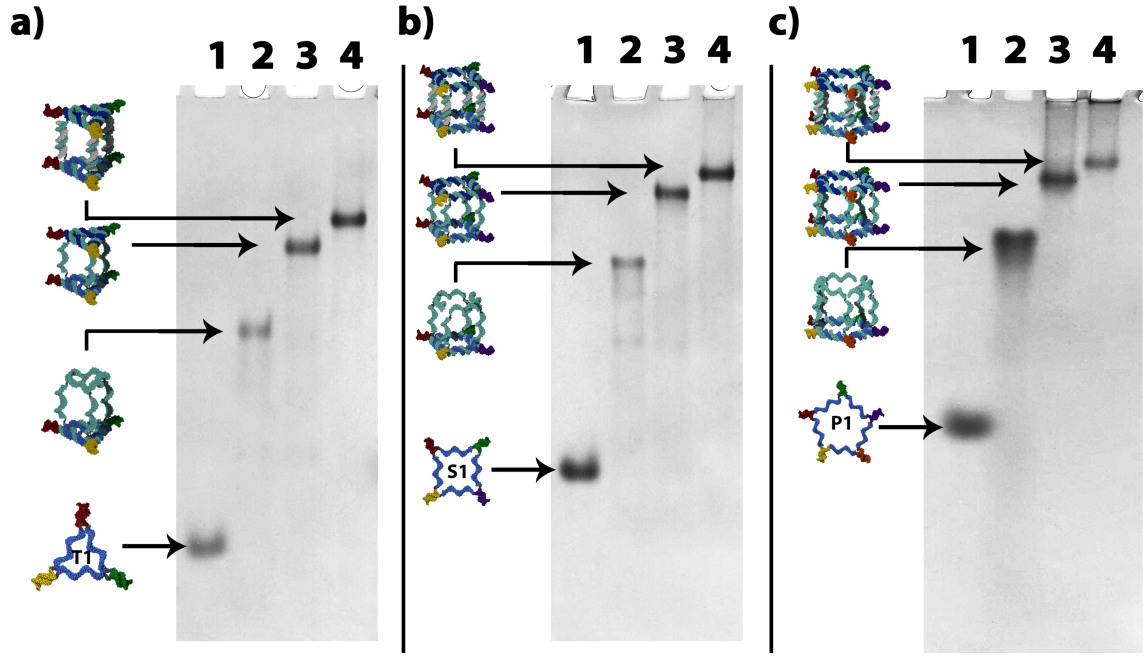

Fig. S4 Modular assembly and PAGE analysis of a) **TP**, b) **RP** and c) **PP**.

The yield of the hexagonal prism **HP** was somewhat reduced as compared to the other cages (Fig. S5b, Lane 2). To more clearly understand 3D assembly using hexagons, we generated a series of 2D derivatives that contained a ten-thymine (T10) sequence where *LS1* would normally bind (Fig. S5a). This effectively knocks out hybridization to *LS1* wherever the T10 tracts are placed within the hexagon structure. The modular way in which 2D polygons are generated allowed us to additionally place T10 sequences in a well-defined orientation, making it easier to examine the effects on 3D assembly. As shown in Fig. S5a, each new hexagon, **H3**-**H7**, was prepared with anywhere from 1-3 T10 sequences. It should be noted that the binding sequence that is retained in each of the modified hexagons is identical to the sequence used in **H1**. Hexagons were assembled in a similar manner as described in Section IV.

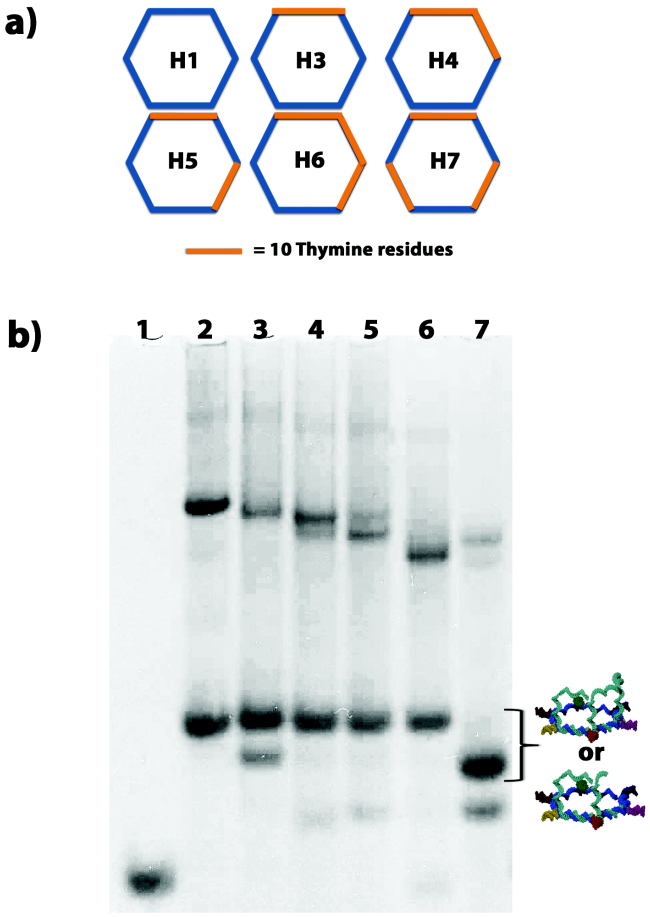

Fig. S5 a) Schematic representation of hexagons that are designed to have 10 thymine (T10) residues that replace the binding sites that interact with linking strand **LS**. b) Lane 1- **H1**, Lane 2- **H1** + *LS1* + **H2**, Lane 3- **H3** + *LS1* + **H2**, Lane 4- **H4** + *LS1* + **H2**, Lane 5– **H5** + *LS1* + **H2**, Lane 6 - **H6** + *LS1* + **H2** and Lane 7 - **H7** + *LS1* + **H2**.

As shown in Fig. S5b, 3D assembly using each hexagon pair results in a distribution of products as analyzed by PAGE under native conditions. In each of Lanes 2-8 there appears to be a distribution between the slower moving 3D products and what appears to be a hexagon with a specific number of linking strands bound to it (schematically represented on the side of the gel). Despite removing half of the binding sites in an effort to reduce steric crowding, as is the case with **H6** (Lane 6) and **H7** (Lane 7), addition of **H2** still results in poor 3D product formation. We hypothesize that despite the pre-organization of the linking strands within each hexagon structure, sterics may still be playing a role upon addition of the second hexagon **H2**. In addition, **H2** contains 6 potential binding sites for the pre-organized linking strands to coordinate with, potentially making it difficult for a single orientation to be preferred. This could result in initial assembly errors that both destabilize the structure and prevent correct orientation of the linking strands. There also appears to be no hexagon starting materials left over in Lanes 2-8, indicating that initial assemblies were indeed formed. Errors in *LS1* binding likely destabilized some of the structures leading to an 'opening up' of some 3D products.

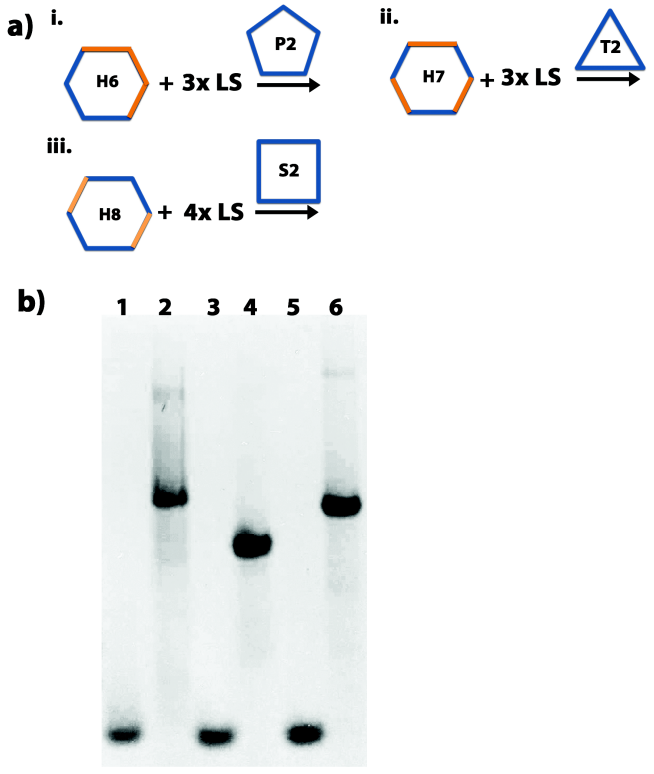

Fig. S6 a) Schematic representation of hexagons that can be assembled into heteroprisms using selective coordination of *LS1* and a second set of polygons, **T2**, **S2**, and **P2**. b) Lane 1- **H6**, Lane 2- **H6** + 3 eqv *LS1* + **P2**, Lane 3- **H7**, Lane 4 – **H7** + 3 eqv *LS1* + **T2**, Lane 5 – **H8** and Lane 6 – **H8** + 4 eqv *LS1* + **S2**.

To test whether the number of binding sites on the 2nd polygon face would impact product yields by contributing to possible errors in assembly, 3D preparation was performed using **P2**, **T2** and **S2** instead of **H2**. Each assembly experiment is schematically represented in Fig. S6a and would formally allow the preparation of heteroprisms that contain a number of different geometries. In Fig. 6a-i, hexagon **H6** is designed to bind three adjacent linking strands that could possibly coordinate to available sites on **P2**. Similarly, the design of **H7** (Fig.6a-ii) and **H8** (Fig. 6a-iii) make it possible to coordinate triangle **T2** and square **S2**, respectively. These experiments reveal that the number of available coordination sites on the 2nd polygon is important in determining how effectively the pre-organized linking strands can bind to yield the closed prismatic structure. Interestingly, pentagon **P2**, which contains five binding sites, assembles well with the pre-organized **H6**. There appears then to be a mechanistic change when going from 6 to 5 binding sites that reduces initial errors in assembly. Thus, tuning the linking strand orientation on each hexagon through selective incorporation of thymine residues allowed us to generate a scaffold that can be used to coordinate other DNA polygons. Such heteroprisms could be additionally modified due to the remaining single-stranded regions. Further investigations are underway to modify **H2** in a manner that will promote efficient assembly of hexagonal prismatic structures.

VI. Characterization of 3D constructs using selective enzymatic digestions

Enzymatic protocols used to carry out the characterization of **TP** and **RP** were performed as previously reported[S1-S3]. The closed, cyclic connectivity of each 3D prism was confirmed using Exonuclease VII (ExoVII) digestion. ExoVII is selective for the digestion of single-stranded open DNA, over that of cyclic closed DNA.[S1,S2] In a typical experiment 0.05 nmoles of DNA (total), was placed in 10 uL of TAEMg buffer and subjected to 5 U of ExoVII at 15 °C for 2 hrs. In addition to ExoVII treatment, the connectivity of 3D constructs **TP, RP** and **PP**, and their respective single-stranded intermediates **ssTP, ssRP** and **ssPP**, was further confirmed using mung bean nuclease (MBN). MBN is selective for the digestion of single-stranded DNA over double-stranded DNA by a factor of 30,000.[S3] Digestions were again performed as previously reported by addition of 20U of MBN to 0.05 nmoles of DNA (total) in a 1xTAEMg buffer system and allowing the digestion to proceed for 2 hr at 15 °C. **ssTP** (lane 1) remains intact after digestion with ExoVII (lane 2) but is digested with MBN (lane 3) due to the single-stranded regions that

comprise the middle portion of prismatic structure. As shown in Fig. S7a, **TP** (lane 4) also remains undigested after ExoVII treatment (lane 5) but is further stabilized against MBN addition (lane 6) due to the double-stranded nature of the sequences that connect the prismatic faces. Similar results were obtained for **ssRP** (Figure S7b lanes, 1- 3) and **RP** (Figure S7b, lanes 4-6), as well as **ssPP** (Figure S7c, lanes 1-3) and **PP** (Figure S7c, lanes 4-6) after nuclease treatment, showing the correct connectivity.

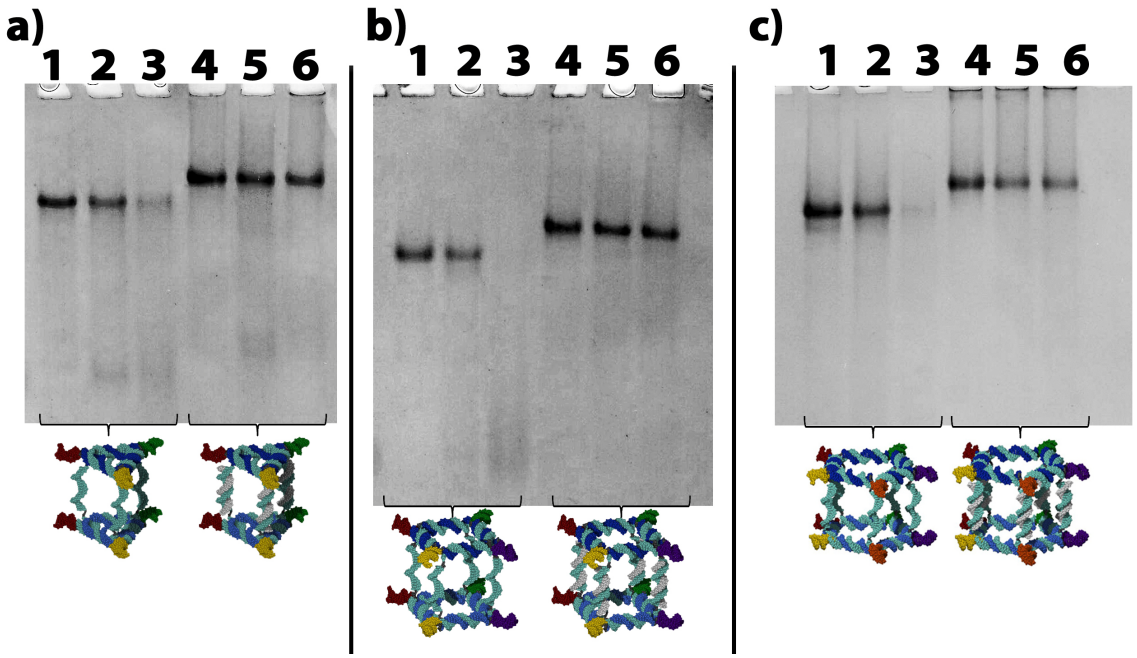

Fig. S7 Connectivity analysis of TP, RP and PP using nucleases ExoVII and MBN. a) **ssTP** (lane 1) was subjected to treatment with ExoVII (lane 2) and MBN (lane 3). Similar analysis was performed on **TP** (lane 4-no enzyme, lane 5- ExoVII, lane 6- MBN). b) The connectivity of second 3D construct **RP** was analyzed using similar enzymatic protocols: **ssRP** (lane 1-no enzyme, lane 2-ExoVII, lane 3- MBN) and **RP** (lane 4-no enzyme, lane 5-ExoVII, lane 6- MBN). c) Enzymatic protocols repeated on the final structures **ssPP** (lane 1-no enzyme, lane 2-ExoVII, lane 3-MBN) and **PP** (lane 4-no enzyme, lane 5-ExoVII, lane 6-MBN).

VII. Characterization of Cooperativity in 3D DNA Assembly

Although it became evident that inclusion of symmetry into the construction strategy was compatible with near quantitative 3D formation of **TP**, **RP**, and **PP**, its presence adds a new facet to the mechanism of assembly. The same *LS1* now acts on all template edges, opening

up the possibility for product formation at less than stoichiometric *LS1* ratios, which could also be the result of a cooperative assembly pathway. To expand on the experiments outlined in the manuscript, *LS1* was added prior to the addition of **T2** to determine whether the individual binding strengths of the two polygons would play a role in determining the extent of cooperative behaviour.

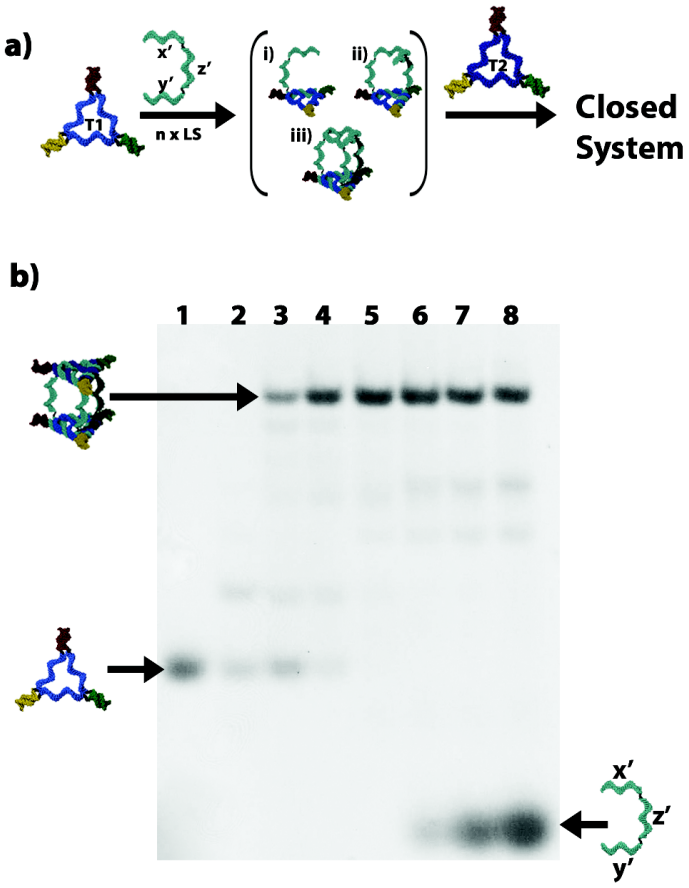

Fig. S8 a) Schematic representation of the assembly of 3D prisms by pre-coordination of various equivalents of *LS1* to **T1** followed by the addition of **T2**. b) Products analyzed by PAGE under native conditions from addition of *LS1* to **T1**, followed by addition of **T2**. In Lanes 1-8 only the number of equivalents of *LS1* are changed. Lane 1- 0 *LS1* eqv, Lane 2 – 0.5 *LS1*, Lane 3 – 1 *LS1*, Lane 4 – 2 *LS1*, Lane 5 – 3 *LS1*, Lane 6 – 6 *LS1*, Lane 7 – 12 *LS1*, Lane 8 – 18 *LS1*.

As shown in Fig. S8a, a given ratio of *LS1* should yield a full distribution of products, **i-iii**, that are pre-organized to bind **T2** to create bi-facial structures. Thus, even with less than a stochiometric amount of *LS1* (n<3), the full prismatic structure could form. Alternatively, when the amounts of *L1S* in solution are n > 3, one could envisage a range of products, unless

selective binding to the second polygon takes place. To explore this potential disproportionation, we added various equivalents of *LS1* to the starting template **T1**, followed by **T2** addition and analysis of the product distributions by PAGE (Fig. S8b). In all experiments where the equivalents of *LS1* are changed from 0.5 – 18 (Fig. S8b, Lanes 2-8) the major product observed is the 3D prism **ssTP**. These results closly mirror those outlined in the manuscript and indicate that subtle differences in the energetics of the single-stranded interior binding regions of the polygons result in a preference for *LS1* coordination at **T1** rather than **T2**. Although difficult to elucidate the cooperative contributions to the 3D assembly mechanism, it can be noted that structure **iii** in Fig. S8a represents a stable prismatic intermediate, suggesting that products with maximal linking strands content are favoured by this face-centered assembly method. In addition, the highly pre-organized nature of this intermediate allows successful binding of the second polygon even in the presence of excess linking strands, making it a selective chelate for 3D prismatic formation.

The selectivity of the pre-organized intermediate, and its ability to form a stable 3D structure, could be further probed by inserting mismatch base pairs into the linking strand binding regions. As shown in the Fig. 1a below, the binding region y′ on the **LS1**, which is responsible for connecting to **T2**, has been site-specifically changed to include either one (**LS$_{y'1}$**) or two (**LS$_{y''2}$**) mismatches. The sequence x, that connects to **T1**, remains the same. In this manner the linking strand would bind properly to **T1** to create the 3-pronged intermediate, shown after step i in Fig. S9a, that is organized to assemble **T2** into the closed 3D structure. The resulting products for each of the different linking strands are shown in Fig. 1b. With no mismatches (**LS1**), the single-stranded triangular prism is assembled (**ssTP**, lane 3). Interestingly, 3D assembly using a linking strand with a single mismatch, **LS$_{y'1}$**, results in a relatively clean product formation (lane 4). With 2 mismatches, **LS$_{y'2}$**, no 3D product is observed (Lane 5). Although a 3D product is observed in the case of the single-mismatch, this product is degraded by ExoVII (Fig. S9c, Lane 4). These experiments indicate that, while the assembly method is partially tolerant to a single-mismatch in the sequence design, the products are not stable in solution.

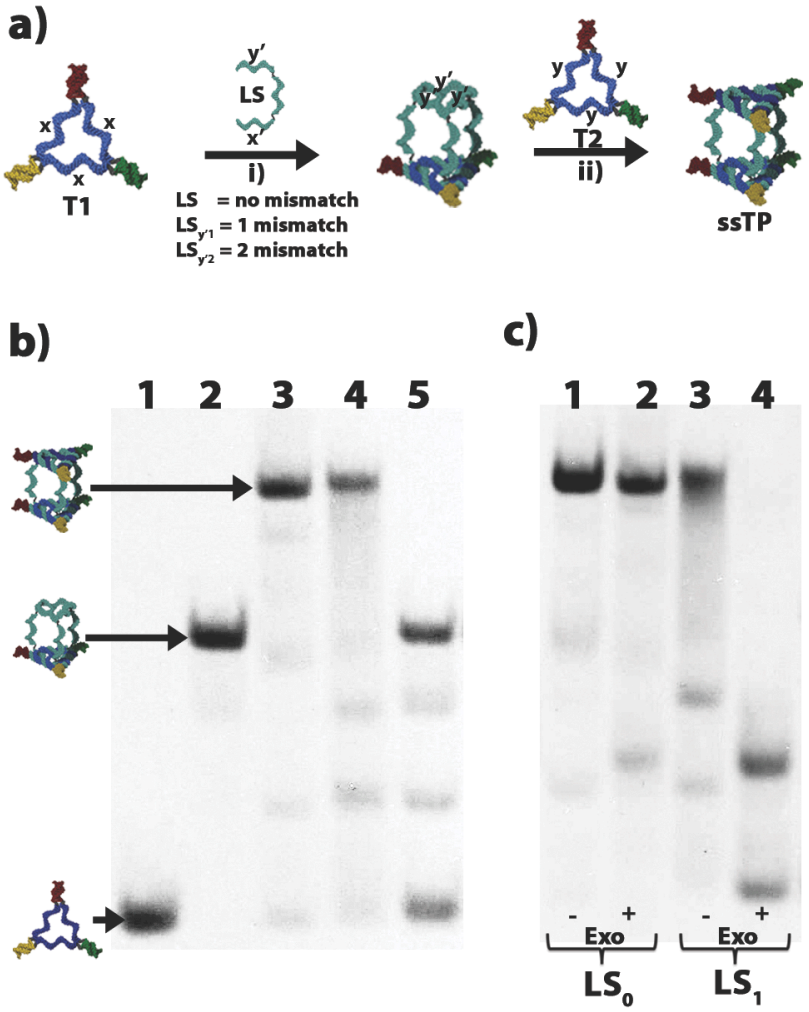

Fig. S9 Incorporation of mismatches into linking strand **LS1** and 3D assembly. a) Schematic repreentation of 3D assembly using linking strands modified to contain mismatch sequences. b) Native PAGE analysis of **ssTP** assembled using **LS**, **LS$_{y'1}$**, and **LS$_{y'2}$**; Lane 1 – **T1**, Lane 2 – **T1** + **LS**, Lane 3 – **T1** + **LS** + **T2**, Lane 4 – **T1** + **LS$_{y'1}$** + **T2** and Lane 5 - **T1** + **LS$_{y'2}$** + **T2**. c) Native PAGE analysis of 3D products after digestion with ExoVII; Lane 1 – **T1** + **LS** + **T2**, Lane 2 – (**T1** + **LS** + **T2**) + ExoVII, Lane 3 – **T1** + **LS$_{y'1}$** + **T2** and Lane 4 – (**T1** + **LS$_{y'1}$** + **T2**) + ExoVII.

VIII. Increasing Symmetry Elements in 3D Assembly

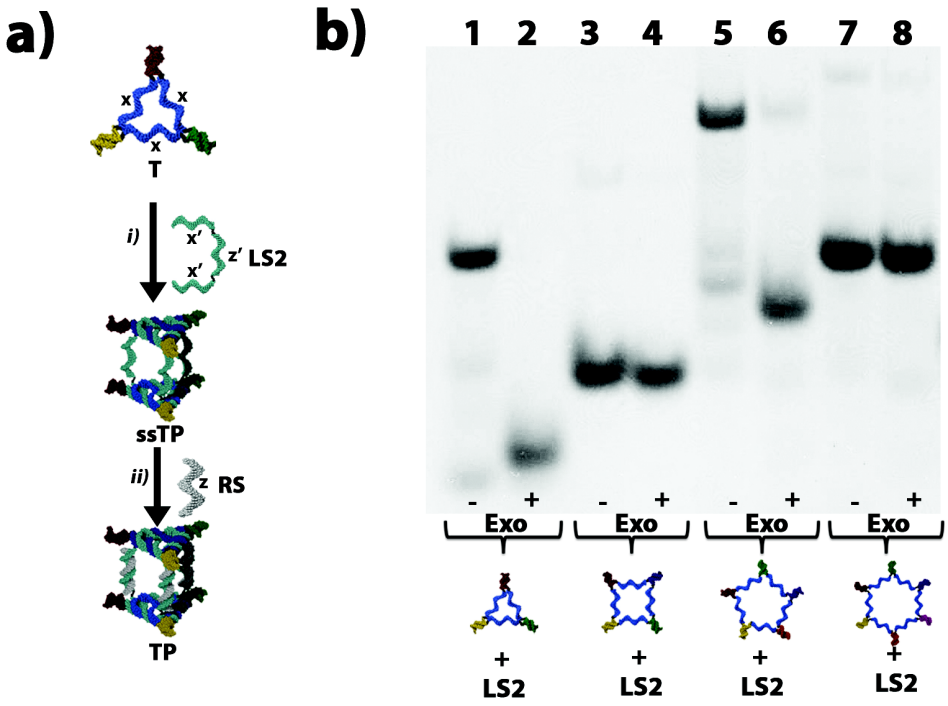

Fig. S10 a) Schematic representation of proposed 3D assembly for **TP** using additional symmetry elements. b) Products analyzed by PAGE under native conditions from addition of *LS2* to **T1**, **S1**, **P1** and **H1** before and after the addition of exonuclease VII (ExoVII). Lane 1- **T1** + *LS2*, Lane 2 – **T1** + *LS2* + ExoVII, Lane 3- **S1** + *LS2*, Lane 4 – **S1** + *LS2* + ExoVII, Lane 5- **P1** + *LS2*, Lane 6 – **P1** + *LS2* + ExoVII, Lane 7 - **H1** + *LS2* and Lane 8 – **H1** + *LS2* + ExoVII.

Additional symmetry was added to our 3D assembly method by designing a linking strand that displays identical 10 base sequences capable of binding polygons **T1**, **S1**, **P1**, and **H1**. This method of assembly would formally produce 3D architectures with pseudo-D_{nh} symmetry. For example, triangular prisms could be assembled to have D_{3h} symmetry as outlined in Fig. S10a. As described in the manuscript, the symmetric linking strand *LS2* can bind intramolecularly to each polygon as opposed to hybridizing with a second face to form linked prismatic structures. Our preliminary assessment of this binding process shows that in cases where there are an even number of available single-stranded regions (**S1** and **H1**), only the intramolecular products are formed. In polygons with an odd number of binding sites (**T1** and **P1**), intramolecular *LS2* hybridization also occurs, but an additional strand then uses the vacant DNA sequence to join two polygons. Enzymatic digestions with ExoVII (as described in Section VI) were performed on the assembled structures obtained from addition of *LS2* to **T1**, **S1**, **P1**, and **H1** (Fig. S10b). With **T1** and **P1** (Lanes 1 and 5), the products of reduced mobility are similar to what was observed for

formation of **ssTp** and **ssPP** (see manuscript). These structures, though, are susceptible to enzymatic degradation (Lanes 2 and 6, respectively). Products obtained from assembly of **S1** and **H1** with *LS2*, however, display much faster mobilities by PAGE (Lanes 3 and 7, respectively) and resist ExoVII digestion (Lanes 4 and 8, respectively). These results indicate that the proposed intramolecular binding process using a symmetric linking strand creates stable closed products. In the case of **T1** and **P1**, the interaction between the two polygons is likely weak, causing the equilibrium in solution to favour a construct with only a single linking strand bound to the remaining binding site on a polygon. This structure would be accessible for ExoVII degradation, unlike in the case of **S1** and **H1** where all regions are occupied by linking strands and leave no points of attack for the enzyme. Additionally, we are further studying the exact structure of each intramolecular product to determine where and how the linking strand is oriented on each 2D polygon. Initial schematic representations of some of the possible binding modes for each polygon are provided in Fig. S11.

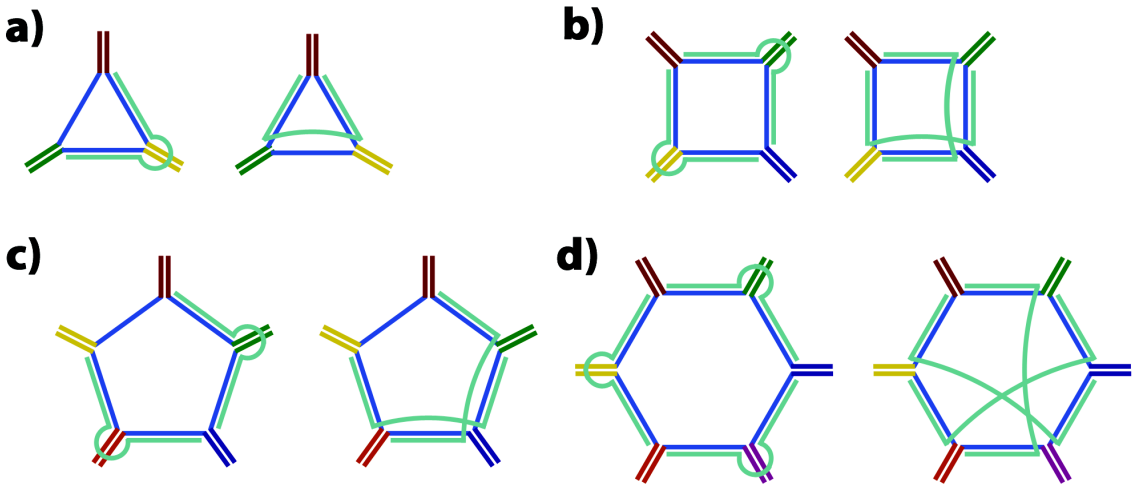

Fig. S11 Schematic representations of intramolecular products from *LS2* assembly for a) **T1**, b) **S1**, c) **P1** and d) **H1**.

To further demonstrate that the intramolecular process was likely competing with intermolecular association of the prismatic faces, we designed a third triangle, **T3**, with a different unique sequence on the interior as compared to **T1** and **T2** (see Section III for sequence details). Because the 10-base duplexes that allow for polygon formation remain the same between each of the three triangles, we could now create an authentic sample of what we propose is two triangles, each with a single intramolecular linking strand, bound together by an additional linking strand that connects the vacant sites on the polygons. This design is schematically represented in Fig S12a. Normal **T1**, with sequences shown in blue, can bind *LS2* to create an architecture with an open binding site. We next designed **T3**, which contains a single component from **T1** (T1a) and two strands from **T2** (T2a and T2b). By designing a new symmetric linking stand *LS3* that is selective for hybridization to the T2a and T2b sequences of this new triangle, we can create a triangle where the empty binding site is now specific to *LS2*. Similarly, with a new set of sequences, T3a-c, we could create another triangle **T4** that contains an *LS2* binding site (from T1a) and two identical sites from T3b and T3c. A final symmetric linking strand *LS4* was created to coordinate these sequences in a intramolecular fashion.

Addition of *LS3* and *LS4* to **T3** and **T4**, respectively, resulted in single bands as observed by PAGE analysis under native conditions (Fig. S12b, Lanes 1 and 2). Typically, with the asymmetric linking strand *LS1*, addition to the triangle results in either the fully loaded construct (Lane 4) or a triangle with 2 linking strands bound (Lane 5). Of note for the products obtained

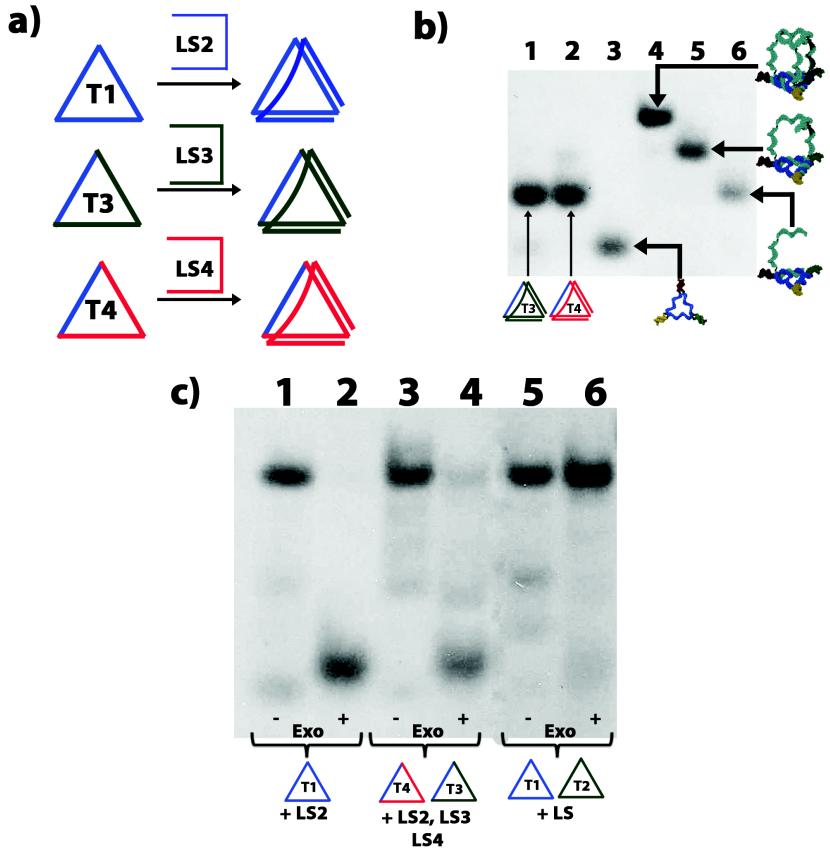

Fig. S12 a) Schematic representation of triangles used to assemble intramolecular products. b) Products analyzed by PAGE under native conditions. Lane 1 – **T3** + *LS3*, Lane 2 – **T4** + *LS4*, Lane 3 – **T1**, Lane 4 – **T1** + *LS1*, Lane 5 – **T5** + *LS1*, Lane 6 – **T6** + *LS1*. c) Products analyzed by PAGE under native conditions before and after ExoVII treatment. Lane 1 – **T1** + *LS2*, Lane 2 – **T1** + *LS2* + ExoVII, Lane 3 – (**T3** + *LS3*) + (**T4** + *LS4*) + *LS2*, Lane 3 – (**T3** + *LS3*) + (**T4** + *LS4*) + *LS2* + ExoVII, Lane 5 – **T1** + *LS1* + **T2** and Lane 6 – **T1** + *LS1* + **T2** + ExoVII.

from **T3** and **T4** is that these bands run slightly slower than a triangle itself (Lane 3) and display migration that is similar to a triangle with only one linking strand bound (Lane 6). Migration and homogeneity of these assembled structures suggests the formation of a single architecture with an intramoelcularly bound linking strand as opposed an arrangement where single-stranded regions are accessible for further binding. To further confirm our assessment, we performed assembly and enzymatic studies using both symmetric and asymmetric methods as shown in Figure S12c. Addition of *LS2* to **T1** again generates a band of slower mobility (Lane 1) that is degraded by ExoVII (Lane 2). An authentic sample of this previous product was then prepared by taking mixtures of **T3**/*LS3* and **T4**/*LS4* and adding *LS2* to link them. A product with identical mobility by PAGE was observed (Lane 3) and similarly underwent degradation after ExoVII treatment

(Lane 4). Interestingly, preparation of **ssTP** using asymmetric linking strand *LS* and triangles **T1** and **T2** results in a band with identical mobility (Lane 5) as observed for the symmetric products, but resists ExoVII degradation (Lane 6). Although formal isomers of each other, each set of products displays a similar mobility by PAGE analysis. The ExoVII results, though, clearly indicate instability of the products obtained by using an additional component of symmetry and further suggest the prominence of an intramolecular mechanism that eliminates intermolecular binding between polygons. Additional studies are underway to elucidate the intramolecular binding process and characterize the unique products formed.

IX. References

S1. See manuscript references 10 and 11.

S2. Kroeker, W. D.; Kowalski, D.; Laskowski, M. Sr. Mung bean nuclease I. Terminally directed hydrolysis of native DNA. *Biochemistry* **15**, 4463-4467 (1976).

S3. Johnson, P. H.; & Laskowski, M. Sr. Mung Bean Nuclease I. II. Resistance of double stranded deoxyribonucleic acid and susceptibility of regions rich in adenosine and thymidine to enzymatic hydrolysis. *J. Biol. Chem.*, **245**, 891 – 898 (1970).